Facile fabrication of WO_3 crystalline nanoplate on FTO glass and their application in electrochromism

Jia Chu[1] ✉, *Jinpeng Lan*[1], *Dengyu Lu*[1], *Jing Ma*[2], *Xiaoqin Wang*[1], *Bohua Wu*[1], *Ming Gong*[1], *Runlan Zhang*[1], *Shanxin Xiong*[1]

[1]*College of Chemistry and Chemical Engineering, Xi'an University of Science and Technology, Xi'an 710054, People's Republic of China*
[2]*School of Metallurgical Engineering, Xi'an University of Architecture and Technology, Xi'an 710055, People's Republic of China*
✉ *E-mail: chujia@xust.edu.cn*

Published in Micro & Nano Letters; Received on 15th April 2016; Revised on 23rd July 2016; Accepted on 25th July 2016

Tungsten trioxide (WO_3) thin films are of great interest as counter electrodes in electrochromic (EC) devices such as 'smart window' for energy-efficient buildings. Uniform WO_3 nanoplates filmed as EC working electrodes were fabricated on seed-free fluorine-tin-oxide (FTO) coated glass via a facile and addictive agent-free hydrothermal process. The WO_3 nanoplates were characterised by scanning electron microscopy and the X-ray photoelectron spectroscopy. The morphological analysis of the film showed that the WO_3 nanoplates lying on the FTO glass uniformly. Fourier transform infrared spectroscopy was applied to study the vibrational information of the sample. Furthermore, uniform WO_3 nanoplates exhibit well performance of EC properties. Owing to the highly two-dimensional nanostructure, a fast switching speed of 12 and 3 s for colouration and bleaching are achieved for WO_3 film. These properties of the WO_3 nanoplates film endow its promising practical applications in smart windows.

1. Introduction: Tungsten trioxide (WO_3) has attracted great interest in various fields such as photocatalysis [1, 2], water splitting [3], supercapacitor [4, 5], lithium-ion batteries [6, 7], gas sensors [8, 9] and electrochromic (EC) [10–12]. Currently, nanostructured WO_3 transition metal oxide has been widely used in EC display devices such as EC windows, high contrast displays, sunroofs, anti-glare mirrors and spacecraft thermal control [13–19]. Especially, EC smart windows have attracted increasing amounts of attention for their great advantages in low-energy consumption, high contrast ratio and good stability. WO_3 can reversibly change from one coloured state to another on supplying a suitable charge, which makes it a promising candidate for smart window. Owing to its low-power consumption and high colour contrast, relatively easy synthesis and low cost, WO_3 has been regarded as the most promising EC material.

Recently, much research has been focused on synthesis of nanostructural WO_3. Till now, a series of WO_3 nanoarchitectures have been prepared such as nanorods, nanowires, nanobundles [20–22] etc. It is well known that the electrochemical property of EC materials strongly depends on the structure. Thin films of WO_3 have been created by various physical and chemical methods including pulsed laser deposition [23], chemical vapour deposition [24], electron-beam evaporation [25], radiofrequency sputtering [26], spray pyrolysis [27], sol–gel [28], layer by layer method [29] and solvothermal/hydrothermal synthesis [20–22, 30]. Accordingly, hydrothermal technique is a low cost, environmental friendly approach to prepare WO_3 with different nanostructures. However, most of these routes are relatively complex in the experimental procedure and some methods should use seed layer and addictive agents. For instance, Chen and Feng have synthesised ultra-thin WO_3 sheets by hydrothermal process with urea as assistant agent. These WO_3 sheet exhibited superior photocatalytic activity [31]. Wang and Li fabricated nanoflake WO_3 films via a crystal-seed-assisted hydrothermal method. The film exhibits faster switching speed and larger optical modulation [11]. To get more effective electrical transport continuity and facilitates Li^+ ion intercalation, simple nanostructure growth technique without seed layer and addictive agent is highly desired.

This Letter explores the fabrication of WO_3 nanoplates directly on seed-free substrates using simple hydrothermal technique without other structural directing agent and addictive agent. The WO_3 nanoplates were characterised by X-ray diffraction (XRD), scanning electron microscopy (SEM), X-ray photoelectron spectroscopy (XPS), and Fourier transform infrared spectroscopy (FTIR). In addition, the cyclic voltammetry (CV) test, electrochemical impedance spectroscopy (EIS) and EC performance of the WO_3 films are also discussed.

2. Experimental

2.1. Preparation of WO_3 nanoplates: A hydrothermal process was used for the synthesis of WO_3 directly on fluorine-tin-oxide (FTO) glass similar to previously reported method [32], but with minor modification. The FTO substrates were cleaned with acetone, ethanol, finally rinsed with deionised water and dried in air. About 0.7 mmol $Na_2WO_4{\cdot}2H_2O$ was dissolved in 30 ml of deionised water under continuous stirring. Then, 10 ml of 3 M HCl solution was added slowly into the prepared solution, followed by the addition of 1 mmol $H_2C_2O_4$ into the above mixture. After 10 min of continuous stirring, another 30 ml of water was added. Finally, the resultant solution was transferred to a teflon-lined stainless steel autoclave and the FTO substrate was placed at an angle against the wall of the autoclave with the conductive side facing down. The hydrothermal was conducted at 180°C for 3 h and then cooled overnight. The FTO glass was thoroughly washed with deionised water and dried in ambient air. The WO_3 nanoplate array film was uniformly coated on the FTO glass substrate.

2.2. Characterisation: XRD data for phase analysis was obtained using a Shimadzu 7000S generator and diffractometer with Cu Ka radiation. The morphology of the samples was observed by using a high-resolution SEM (Supra 55, Carl Zeiss, Germany). XPS analyses were performed on a Kratos Axis. FTIR spectrum was collected on a Perkin-Elmer spectrometer. The CV test and EIS were carried out on an electrochemical workstation (Autolab PGSTAT302N) in a three-electrode environment with the WO_3

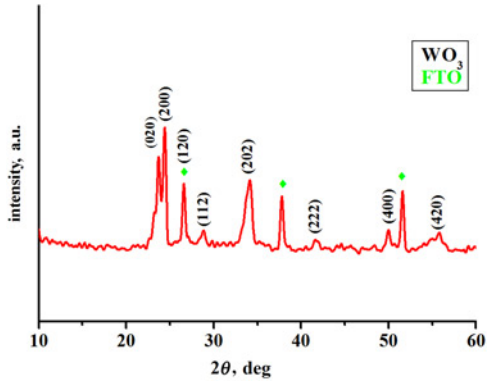

Fig. 1 *XRD patterns of WO_3 nanoplate*

on FTO glass as the working electrode, neat Pt plate as the counter electrode and Ag/AgCl as the reference electrode. About 1 M lithium perchlorate ($LiClO_4$) in propylene carbonate was used as the electrolyte. The EC behaviour of WO_3 films was examined using an Autolab PGSTAT101 potentiostat with the ultraviolet–visible spectrometer (SHIMADZU UV2550).

3. Result and discussion: XRD was employed to analyse the crystal structure and phase properties of the as-prepared WO_3 nanoplates on FTO glass. As shown in Fig. 1, the main diffraction peaks of WO_3 are located at 23.4°, 24.4°, 26.6°, 28.9°, 33.6°, 41.9°, 49.9°, 55.9°, which can be well-indexed to (020), (200), (120), (112), (202), (222), (400), (420) crystal planes of monoclinic phase WO_3 (JCPDS Card No. 83-0950, space group: $P21/n$ with lattice parameters of $a = 7.301$ Å, $b = 7.539$ Å, and $c = 7.689$ Å). The strong peaks indicate the as-prepared WO_3 nanoplates have great crystal quality.

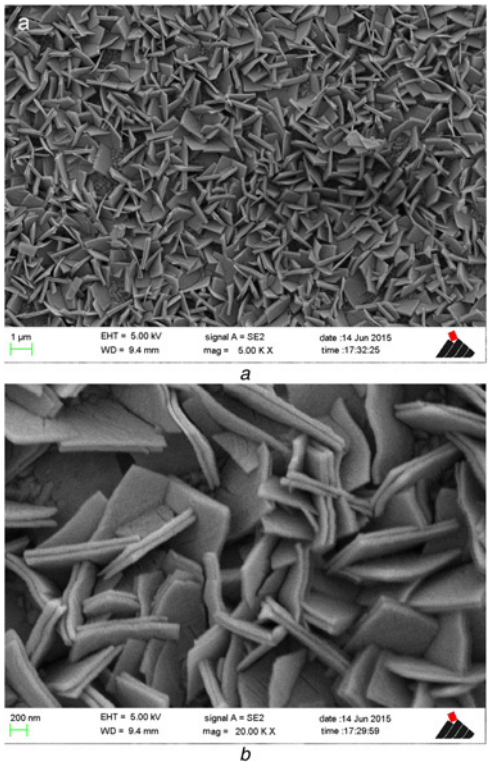

Fig. 2 *SEM images of the WO_3 electrode*
a Low magnification
b Higher magnification

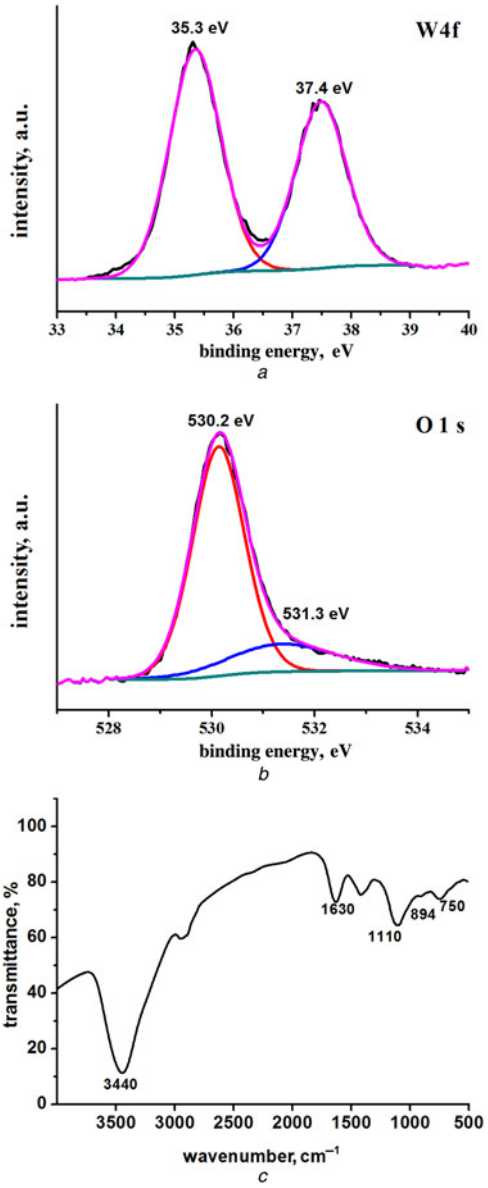

Fig. 3 *XPS survey spectra and FTIR spectrum of WO_3 nanoplates*
a High-resolution XPS spectra of W4f
b High-resolution XPS spectra of O1s
c FTIR spectrum of WO_3 nanoplates

Fig. 2 depicts the SEM images of WO_3 lying on the FTO glass uniformly. Low magnification SEM image of Fig. 2*a* reveals that the product consisted of large quantity of uniform nanoplates. Clearly, the morphology of WO_3 indicates an aggregation of two plates with the same size. Furthermore, an average length and thickness of the platelets determined from the SEM images were around 1.5 μm and 150 nm as shown in Fig. 2*b*.

To estimate the surface composition and chemical status of WO_3 nanoplates, the XPS analysis was carried out and the results are shown in Fig. 3. As depicted in Fig. 3*a*, the peak energies of 34.5 and 37.4 eV are attributed to $W4f_{7/2}$ and $W4f_{5/2}$, respectively, which corresponding to tungsten atoms in a W^{6+} formal oxidation state according to literature [33]. The O 1 s spectrum of WO_3 was shown in Fig. 3*b*. The peak at 530.2 eV corresponds to the formation of W–O–W in WO_3 crystal and the peak 531.3 eV belongs to the −OH or adsorption of water molecules on the surface of the WO_3 [34]. The FTIR spectrum of the as-synthesised WO_3 was recorded in the wavenumber range of 400–4000 cm^{-1} as shown in Fig. 3*c*. The absorption band at 750 cm^{-1} was attributed to the

doi: 10.1049/mnl.2016.0199

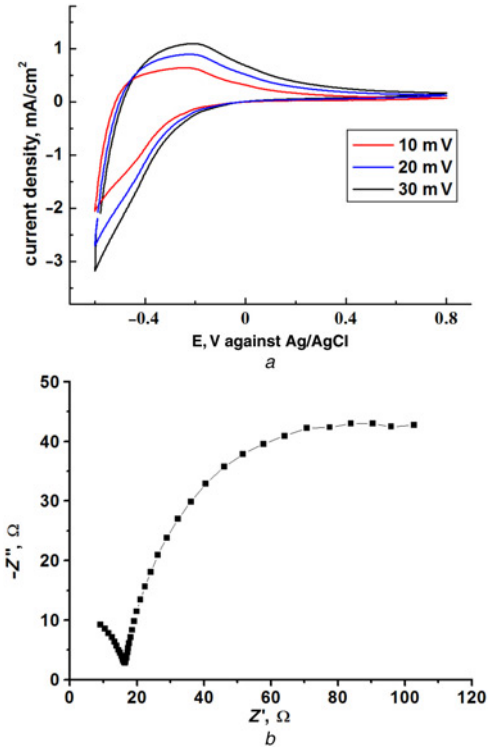

Fig. 4 *CV curves and electrochemical impedance spectrum (Nyquist plots) of WO_3*
a CV curves
b Electrochemical impedance spectrum

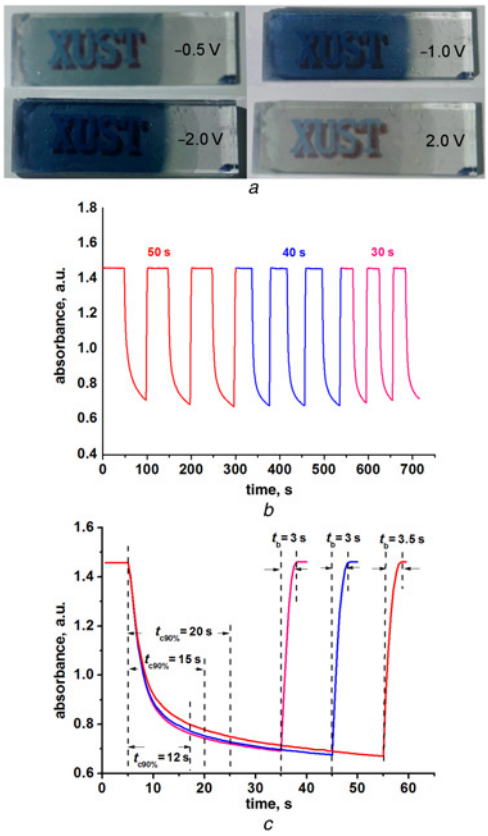

Fig. 5 *Digital photographs of the bleached/coloured WO_3 nanoplate film after applying potentials and switching time characteristics*
a Digital photographs of the bleached/coloured WO_3 nanoplate film
b Different switching time characteristics between the coloured and bleached states for WO_3 film measured at 670 nm, ±2.0 V bias
c Coloured/bleached response time in one switch for WO_3 nanoplate film measured at ±2.0 V for 50 s (red line), 40 s (blue line) and 30 s (pink line) with an absorbance wavelength of 670 nm

corner-sharing mode ν(W–O–W) and the broad bands located around 894 cm^{-1} originate from the vibrations of the O–W–O bridging bond inside the octahedrons. An intensive band around 1110 cm^{-1} was related to the terminal W=O bond for crystalline WO_3 [35]. In addition, the bands at 1630 and 3400 cm^{-1} were indication of hydroxyl groups of hydrous WO_3 vibrations and the stretching vibrations of water molecules adsorbed on the octahedral layer surface.

The electrochemical properties of the as-synthesised WO_3 were studied. Fig. 4*a* shows the CV curves of the WO_3 film, which was recorded between −0.6 and 0.8 V at various scan rates from 10 to 30 mV s^{-1}. The CV curves were attributed to the lithium-ion intercalation into the WO_3 nanoplates electrode and the deintercalation process. As the scan rate is increased, the anodic peaks corresponding to the Li^+ deintercalation gradually shift toward the positive potential. Owing to the layered structure of WO_3 nanoplates, Li^+ cations could be intercalated into/deintercalated out of the structure easily. EIS was conducted to further understand the electrochemical behaviour of the as-prepared WO_3 film as shown in Fig. 4*b*. According to the previous reports [7], the intercept on the *Z*′-axis in the high frequencies region represents the resistance of the electrolyte (R_e); the high-frequency semi-circle can be assigned to the resistance R_f and CPE of the WO_3 film. Normally, the smaller arc radii in Nyquist plot, the better charge transfer ability. It can be seen that the semi-circle of the WO_3 film is small, which contributes to the high electrochemical performance of the WO_3 film.

The EC phenomena of the as-prepared WO_3 nanorod array film were measured using a two-electrode electrochemical cell in a 1.0 M $LiClO_4$–PC electrolyte solution. Fig. 5*a* shows the digital photographs of the WO_3 nanowire array film at different potentials. As revealed in the picture, the WO_3 nanoplates film displays a high contrast between the bleached and coloured states. When applying a potential of −0.5 V, −1.0 V and −2.0 V, the colour of the WO_3 films are slate blue, steel blue and navy blue, respectively, revealing excellent colour reversibility [36]. This process is in accordance with intercalation (deintercalation) of the Li^+ into (out from) the WO_3 films

$$WO_3(\text{bleach}) + xLi^+ + xe^- \longleftrightarrow Li_xWO_3(\text{blue}).$$

The in situ colouration/bleaching absorbance response were investigated at a fixed wavelength of 670 nm. The colouration and bleaching times are defined as the time required for 90% change in the entire absorbance modulation. We measured its absorbance switching characteristic by scanning at ±2.0 V for 30, 40 and 50 s, respectively. As shown in Figs. 5*b* and *c*, when the scanning time is 30 s, the colouration time t_c and bleaching time t_b are found to be 12 and 3 s, respectively, which are faster than those previous reports. The fast switching speed of the WO_3 film is the result of the nanoplate structure, which makes it easier for the Li^+ ion intercalation process to complete. The switching response of the WO_3 thin film under 40 and 50 s are also investigated, as shown in Fig. 5*c*, and the t_c are 15 and 20 s, respectively. On the other hand, the t_b of the film is almost the same under different scanning time. This result agreed well with the EIS measured before, indicating that superior EC activity of the plate-like WO_3 film was mainly attributed to its high efficiency of electron transport.

4. Conclusion: In summary, plate-like WO_3 films are assembled directly on an FTO glass substrate via a facile seed-free hydrothermal method. The structural, electrochemical and EC studies based on this film are presented. The WO_3 film shows good colourations/bleaching switching characteristics, because the

two-dimensional structure of the WO_3 film will provide more effective electrical transport continuity and facilitates Li^+ ion intercalation. There is a good prospect of applying these hydrothermal WO_3 thin films in smart windows and electronic papers.

5. Acknowledgments: This work was supported by the National Natural Science Foundation of China (NSFC, grant nos. 51503169, 51402231 and 21406176) and the Natural Science Foundation of Shaanxi Province (2014JQ2072, 2014JQ2076).

6 References

[1] Hunge Y.M., Mahadik M.A., Kumbhar S.S., *ET AL.*: 'Visible light catalysis of methyl orange using nanostructured WO_3 thin films', *Ceram. Int.*, 2016, **42**, pp. 789–798

[2] Tanaka A., Hashimoto K., Kominami H.: 'Visible-light-induced hydrogen and oxygen formation over Pt/Au/WO_3 photocatalyst utilizing two types of photoabsorption due to surface plasmon resonance and band-gap Excitation', *J. Am. Chem. Soc.*, 2014, **136**, pp. 586–589

[3] Li Y., Wei X., Yan X., *ET AL.*: 'Construction of inorganic-organic 2D/2D WO_3/g-C_3N_4 nanosheet arrays toward efficient photoelectrochemical splitting of natural seawater', *Phys. Chem. Chem. Phys.*, 2016, **4**, pp. 7266–7273

[4] Qiu M., Sun P., Shen L., *ET AL.*: 'WO_3 nanoflowers with excellent pseudo-capacitive performance and the capacitance contribution analysis', *J. Mater. Chem. A*, 2016, doi: 10.1039/C6TA00237D

[5] Zhou Y., Ko S., Lee C.W., *ET AL.*: 'Enhanced charge storage by optimization of pore structure in nanocomposite between ordered mesoporous carbon and nanosized WO_{3-x}', *J. Power Sources*, 2013, **244**, pp. 777–782

[6] Yin J., Cao H., Zhang J., *ET AL.*: 'Synthesis and applications of γ-tungsten oxide hierarchical nanostructures', *Cryst. Growth Des.*, 2013, **13**, pp. 759–769

[7] Gao L., Qu F., Wu X.: 'Hierarchical WO_3@SnO_2 core-shell nanowire arrays on carbon cloth: a new class of anode for high-performance lithium-ion batteries', *J. Mater. Chem. A*, 2014, **2**, pp. 7367–7372

[8] Long H., Zeng W., Zhang H.: 'Synthesis of WO_3 and its gas sensing: a review', *J Mater. Sci., Mater. Electron.*, 2015, **26**, pp. 4698–4707

[9] Garcia-Sanchez R.F., Ahmido T., Casimir D., *ET AL.*: 'Thermal effects associated with the Raman spectroscopy of WO_3 gas-sensor materials', *J. Phys. Chem. A*, 2013, **117**, pp. 13825–13831

[10] Hung C.J., Huang Y.H., Chen C.H., *ET AL.*: 'Hydrothermal formation of tungsten trioxide nanowire networks on seed-free substrates and their properties in electrochromic device', *IEEE Trans. Compon. Packag. Manuf.*, 2014, **4**, pp. 831–839

[11] Ma D., Wang H., Zhang Q., *ET AL.*: 'Self-weaving WO_3 nanoflake films with greatly enhanced electrochromic performance', *J. Mater. Chem.*, 2012, **22**, pp. 16633–16639

[12] Qu H., Zhang X., Pan L., *ET AL.*: 'One-pot preparation of crystalline-amorphous double-layer structured WO_3 films and their electrochromic properties', *Electrochim. Acta*, 2014, **148**, pp. 46–52

[13] Moscovici J., Rougier A., Laruelle S., *ET AL.*: 'Apparent mismatch between extended X-ray absorption fine structure and diffraction structures of crystalline metastable WO_3 phases', *J. Chem. Phys.*, 2006, **125**, p. 124505

[14] Sauvet K., Sauques L., Rougier A.: 'Electrochromic properties of WO_3 as a single layer and in a full device: from the visible to the infrared', *J. Phys. Chem. Solids*, 2010, **71**, pp. 696–699

[15] Aliev A.E., Shin H.W.: 'Image diffusion and cross-talk in passive matrix electrochromic displays', *Displays*, 2002, **23**, pp. 239–247

[16] Baetens R., Jelle B.P., Gustavsen A.: 'Properties, requirements and possibilities of smart windows for dynamic daylight and solar energy control in buildings: a state-of-the-art review', *Sol. Energy Mater. Sol. Cells*, 2010, **94**, pp. 87–105

[17] Alamri S.N.: 'The temperature behavior of smart windows under direct solar radiation', *Sol. Energy Mater. Sol. Cells*, 2009, **93**, pp. 1657–1662

[18] Tajima K., Yamada Y., Bao S.H., *ET AL.*: 'Characterization of flexible switchable mirror film prepared by DC magnetron sputtering', *Vacuum*, 2010, **84**, pp. 1460–1465

[19] Giancaterini L., Emamjomeh S.M., De Marcellis A., *ET AL.*: 'The influence of thermal and visible light activation modes on the NO_2 response of WO_3 nanofibers prepared by electrospinning', *Sens. Actuators B, Chem.*, 2016, **229**, pp. 387–395

[20] Zhang J., Tu J., Xia X., *ET AL.*: 'Hydrothermally synthesized WO_3 nanowire arrays with highly improved electrochromic performance', *J. Mater. Chem.*, 2011, **21**, pp. 5492–5498

[21] Ma D., Shi G., Wang H., *ET AL.*: 'Morphology-tailored synthesis of vertically aligned 1D WO_3 nano-structure films for highly enhanced electrochromic performance', *J. Mater. Chem. A*, 2013, **1**, pp. 684–691

[22] Chang X., Sun S., Li Z., *ET AL.*: 'Assembly of tungsten oxide nanobundles and their electrochromic properties', *Appl. Surf. Sci.*, 2011, **257**, pp. 5726–5730

[23] Rougier A., Portemer F., Quédé A., *ET AL.*: 'Characterization of pulsed laser deposited WO_3 thin films for electrochromic devices', *Appl. Surf. Sci.*, 1999, **153**, pp. 1–9

[24] Houweling Z.S., Geus J.W., Schropp R.E.I.: 'Hot-wire chemical vapor deposition of WO_{3-x} thin films of various oxygen contents', *Mater. Chem. Phys.*, 2013, **140**, pp. 89–96

[25] Madhuri K.V., Babu M.B.: 'Studies on electron beam evaporated WO_3 thin films', *Mater. Today, Proc.*, 2016, **3**, pp. 84–89

[26] Ou J.Z., Balendhran S., Field M.R., *ET AL.*: 'The anodized crystalline WO_3 nanoporous network with enhanced electrochromic properties', *Nanoscale*, 2012, **4**, pp. 5980–5988

[27] O-Rueda de Leona J.M., Acostaa D.R., Palb U., *ET AL.*: 'Improving electrochromic behavior of spray pyrolised WO_3 thin solid films by Mo doping', *Electrochim. Acta*, 2011, **56**, pp. 2599–2605

[28] Wang W., Pang Y., Hodgson N.B.: 'Design and fabrication of bimodal meso-mesoporous WO_3 thin films and their electrochromic properties', *J. Mater. Chem.*, 2010, **20**, pp. 8591–8599

[29] Ling H., Liu L., Lee P.S., *ET AL.*: 'Layer-by-layer assembly of PEDOT:PSS and WO_3 nanoparticles: enhanced electrochromic coloration efficiency and mechanism studies by scanning electrochemical microscopy', *Electrochim. Acta*, 2015, **22**, pp. 57–65

[30] Qin D.D., Tao C.L., Friesen S.A., *ET AL.*: 'Dense layers of vertically oriented WO_3 crystals as anodes for photoelectrochemical water oxidation', *Chem. Commun.*, 2012, **48**, pp. 729–731

[31] Zheng Y., Chen G., Yu Y., *ET AL.*: 'Urea-assisted synthesis of ultrathin hexagonal tungsten trioxide photocatalyst sheets', *J. Mater. Sci.*, 2015, **50**, pp. 8111–8119

[32] Yang J., Li W., Li J., *ET AL.*: 'Hydrothermal synthesis and photoelectrochemical properties of vertically aligned tungsten trioxide (hydrate) plate-like arrays fabricated directly on FTO substrates', *J. Mater. Chem.*, 2012, **22**, pp. 17744–17752

[33] Xie F., Gong L., Liu X., *ET AL.*: 'XPS studies on surface reduction of tungsten oxide nanowire film by Ar^+ bombardment', *J. Electron Spectrosc. Relat. Phenom.*, 2012, **185**, pp. 112–118

[34] Shamaila S., Sajjad A., Chen F., *ET AL.*: 'WO_3/BiOCl, a novel heterojunction as visible light photocatalyst', *J. Colloid Interface Sci.*, 2011, **356**, pp. 465–472

[35] Orel B., Krašovec U.O., Grošelj N., *ET AL.*: 'Gasochromic behavior of sol–gel derived Pd doped peroxopolytungstic acid (W-PTA) nanocomposite films', *J. Sol-Gel Sci. Technol.*, 1999, **14**, pp. 291–308

[36] Jiao Z.H., Sun X.W., Wang J.M., *ET AL.*: 'Hydrothermally grown nanostructured WO_3 films and their electrochromic characteristics', *J. Phys. D, Appl. Phys.*, 2010, **43**, pp. 285501–285506

doi: 10.1049/mnl.2016.0199